Supporting information

A new quaternary sphalerite-derivative compound for thermoelectric applications: Cu_7VSnS_8

Shuya Kozai,[a] Koichiro Suekuni [*ab], Seiya Takahashi[c], Eiji Nishibori[c], Hidetaka Kasai[c], Ilaria Siloi[d,e], Marco Fornari[d], Hikaru Saito[f], Philipp Sauerschnig[g], Michihiro Ohta[g], Pierric Lemoine[h], Emmanuel Guilmeau[i], Bernard Raveau[i], and Michitaka Ohtaki[ab]

a Interdisciplinary Graduate School of Engineering Sciences, Kyushu University, Kasuga, Fukuoka 816-8580, Japan. E-mail: suekuni.koichiro.063@m.kyushu-u.ac.jp

b Transdisciplinary Research and Education Center for Green Technologies, Kyushu University, Kasuga, Fukuoka 816-8580, Japan.

c Faculty of Pure and Applied Sciences and Tsukuba Research Center for Energy Materials Science (TREMS), University of Tsukuba, Tsukuba, 305-8571, Japan.

d Department of Physics and Science of Advanced Materials Program, Central Michigan University, Mt. Pleasant, Michigan 48859, United States.

e Department of Physics and Astronomy, University of Padua, Padova, Italy

f Institute for Materials Chemistry and Engineering, Kyushu University, Kasuga, Fukuoka 816-8580, Japan

g Global Zero Emission Research Center, National Institute of Advanced Industrial Science and Technology (AIST), Tsukuba, Ibaraki 305-8569, Japan.

h Institut Jean Lamour, UMR 7198 CNRS – Université de Lorraine, 54011 Nancy Cedex, France.

i CRISMAT, CNRS, Normandie Université, 14000 Caen, France.

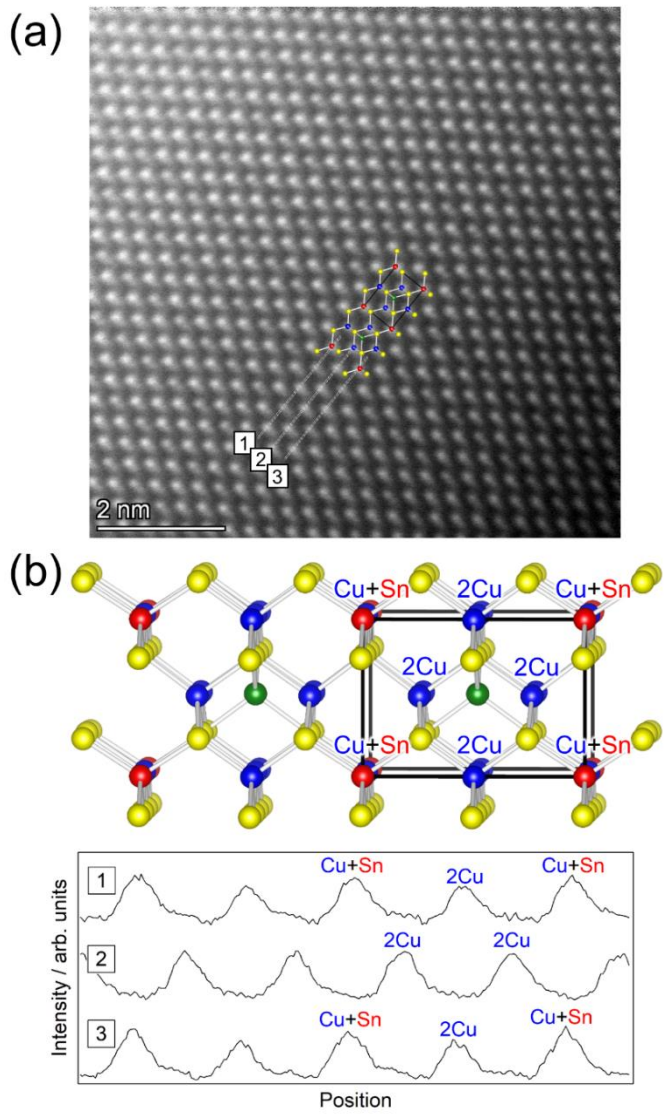

Fig. S1 (a) Annular dark-field scanning transmission electron microscopy image and (b) crystal structure representation of Cu_7VSnS_8 along the *a*-axis. The atomic columns shown in (a) are well aligned and the position and relative intensity of spots are consistent with those expected from the Cu_7VSnS_8 structure. More specifically, (c) the intensities of the Sn-rich columns exhibit higher intensity than Cu columns for line profiles of 1–3 in (a). The labels of the atomic columns (Cu+Sn, 2Cu) represents the number of atoms periodically contained in the columns. It should be noted that the V atom is not visible in the profile, which is supposed to be due to the small atomic number of V and isolated arrangement of V along the *a* axis.

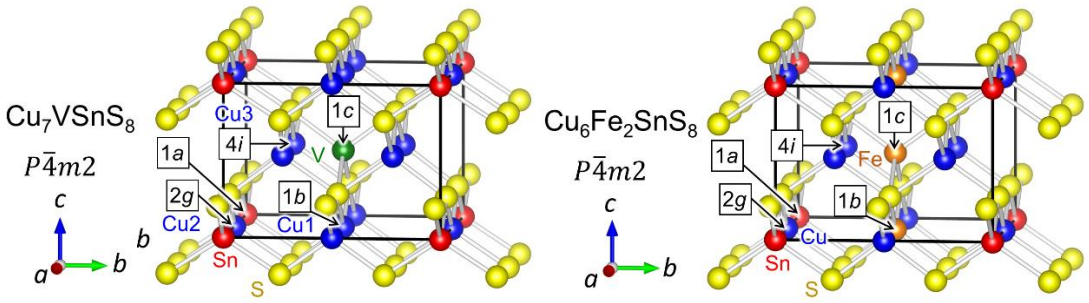

Fig. S2 Crystal structures of Cu_7VSnS_8 and $Cu_6Fe_2SnS_8$ (mawsonite).

Table S1 Crystallographic information of Cu_7VSnS_8 at temperatures between 300 K and 673 K obtained from synchrotron powder X-ray diffraction.

Temp	300 K	373 K	423 K	473 K	523 K	573 K	623 K	673 K
RI	0.03400	0.03840	0.03998	0.04510	0.04840	0.05103	0.05656	0.06158
Rwp	0.04145	0.04082	0.03994	0.04105	0.04212	0.04274	0.04482	0.04796
a/Å	7.59837(5)	7.60606(5)	7.61090 (5)	7.61587(6)	7.62162(6)	7.62782(6)	7.63361(7)	7.63913(7)
c/Å	5.38515(5)	5.39224(5)	5.39682(5)	5.40153(5)	5.40708(6)	5.41305(6)	5.41877(6)	5.42446(6)
Sn *B*/Å^2	0.96(4)	1.21(4)	1.36(4)	1.52(5)	1.66(5)	1.84(5)	2.04(6)	2.16(6)
Cu1 *B*	1.21(5)	1.58(5)	1.81(6)	2.06(6)	2.32(7)	2.55(7)	2.82(8)	3.11(9)
Cu2 *z*	-0.0035(19)	-0.0019(23)	-0.0008(24)	-0.0001(27)	0.0009(27)	0.0025(28)	0.0029(3)	0.0033(3)
Cu2 *B*/Å^2	2.16(4)	2.85(5)	3.30(5)	3.80(6)	4.36(6)	4.98(7)	5.63(7)	6.18(9)
Cu3 *x*	0.2466(3)	0.2464(3)	0.2463(3)	0.2463(3)	0.2461(3)	0.2456(3)	0.2454(3)	0.2452(4)
Cu3 *B*/Å^2	1.28(3)	1.61(3)	1.85(3)	2.10(4)	2.39(4)	2.76(4)	3.04(5)	3.34(5)
V *B*/Å^2	0.75(5)	0.97(6)	1.04(6)	1.20(7)	1.37(7)	1.50(8)	1.63(9)	1.83(10)
S1 *x*	0.2562(4)	0.2558(5)	0.2558(4)	0.2560(4)	0.2559(5)	0.2556(6)	0.2554(5)	0.2555(5)
S1 *z*	0.2382(6)	0.2370(6)	0.2367(6)	0.2364(6)	0.2368(6)	0.2371(7)	0.2371(7)	0.2374(8)
S1 *B*/Å^2	0.64(9)	0.69(8)	0.84(9)	1.06(10)	1.15(11)	1.45(13)	1.48(13)	1.63(14)
S2 *x*	0.2564(5)	0.2563(5)	0.2568(5)	0.2570(4)	0.2573(5)	0.2569(5)	0.2573(5)	0.2574(5)
S2 *z*	0.2463(7)	0.2442(7)	0.2438(7)	0.2429(7)	0.2430(7)	0.2434(7)	0.2429(7)	0.2423(8)
S2 *B*/Å^2	1.40(11)	1.73(11)	1.86(12)	1.96(13)	2.26(14)	2.37(16)	2.65(17)	2.86(18)

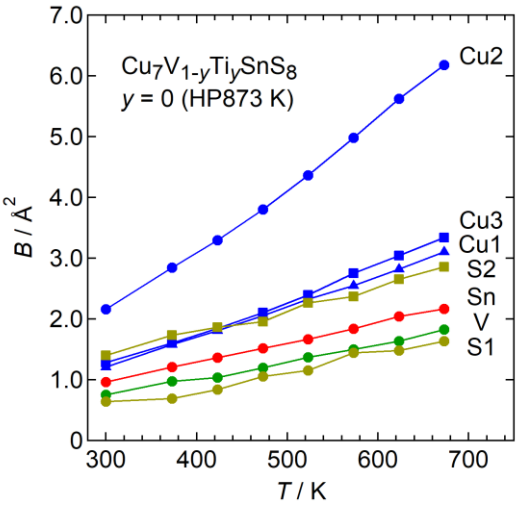

Fig. S3 Isotropic thermal parameter of atoms for Cu_7VSnS_8. The values are summarized in Table S1.

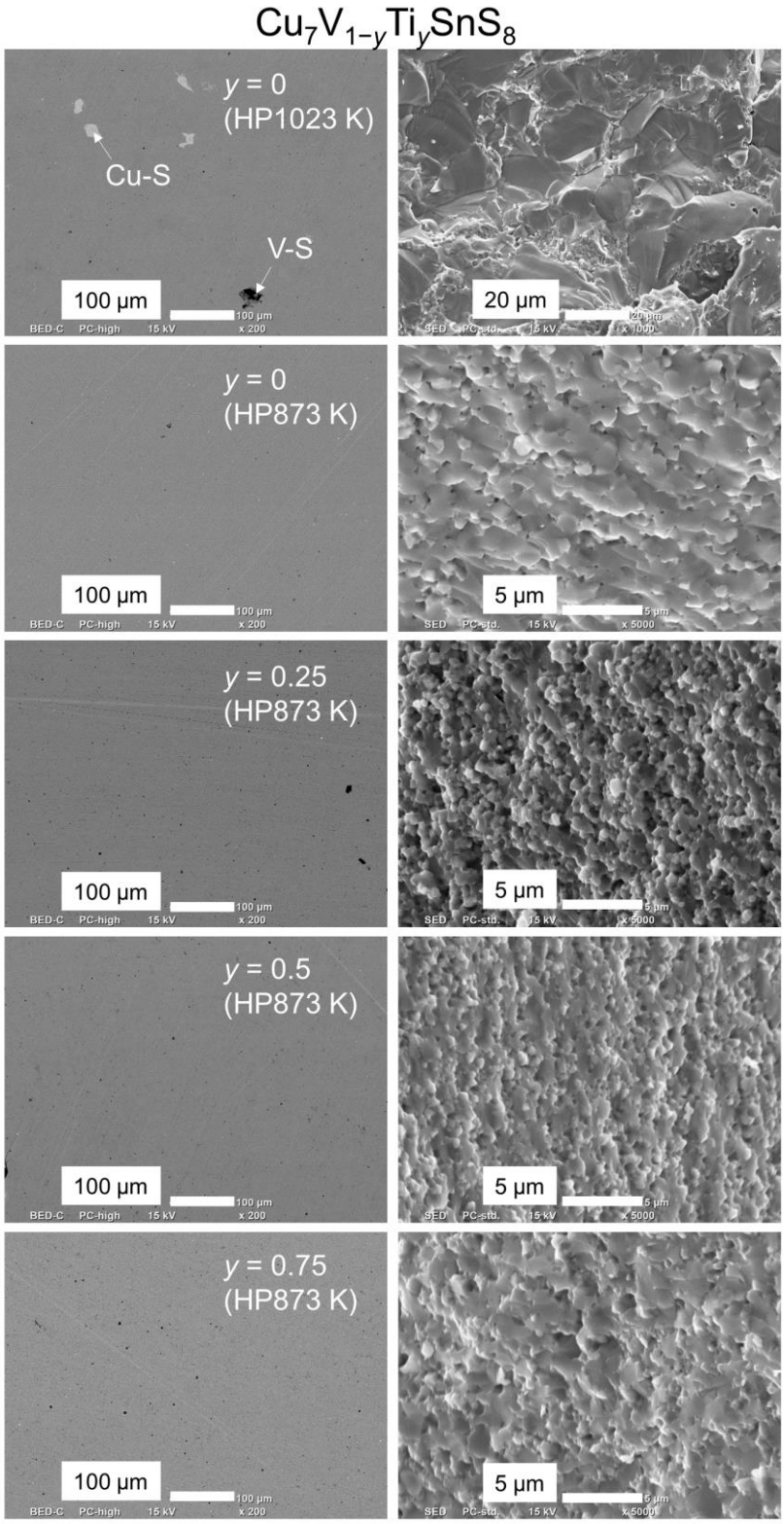

Fig. S4 Backscattered electron images for the polished surfaces and secondary electron images for the fractured surfaces of the hot-pressed samples of $Cu_7V_{1-y}Ti_ySnS_8$ (y = 0–0.75).

Table S2 Hot-press temperature and chemical composition of $Cu_7V_{1-y}Ti_ySnS_8$ (y = 0–0.75). The compositions were obtained by averaging the energy dispersive X-ray spectroscopy data for 20 randomly selected spots. Here, the total composition of Cu, Ti, V, and Sn are assumed to be 9.

y	HP Temp.	Cu	Ti	V	Sn	S
0	1023	7.00(11)	—	0.97(6)	1.03(5)	7.3(3)
0	873	6.94(4)	—	1.00(3)	1.05(2)	7.54(9)
0.25	873	6.98(4)	0.23(2)	0.75(3)	1.05(2)	7.43(9)
0.5	873	6.98(4)	0.48(3)	0.50(3)	1.05(2)	7.41(9)
0.75	873	6.95(4)	0.73(2)	0.25(2)	1.07(3)	7.42(7)

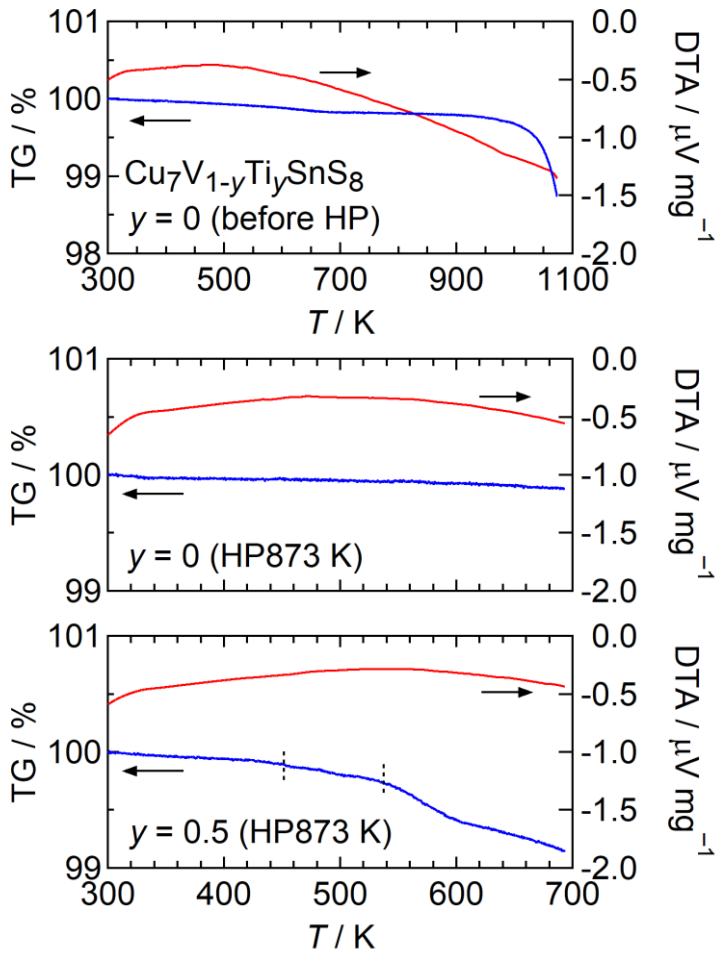

Fig. S5 Thermogravimetry/differential thermal analysis data for the powdered samples of $Cu_7V_{1-y}Ti_ySnS_8$ (y = 0, 0.5).

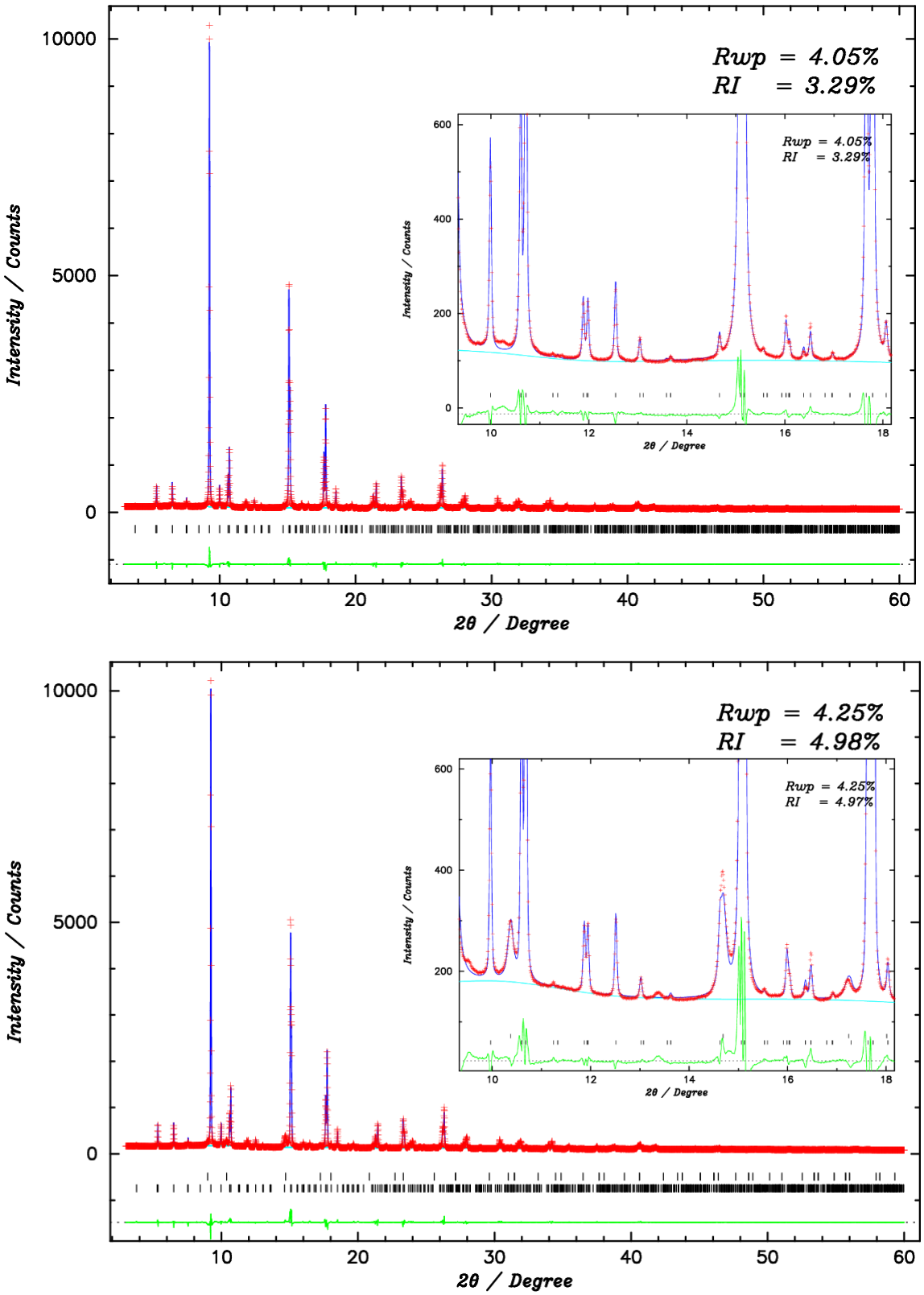

Fig. S6 Synchrotron powder X-ray diffraction patterns for the sample of $Cu_7V_{1-y}Ti_ySnS_8$ (y = 0.5) at 300 K before and after heating up to 673 K.

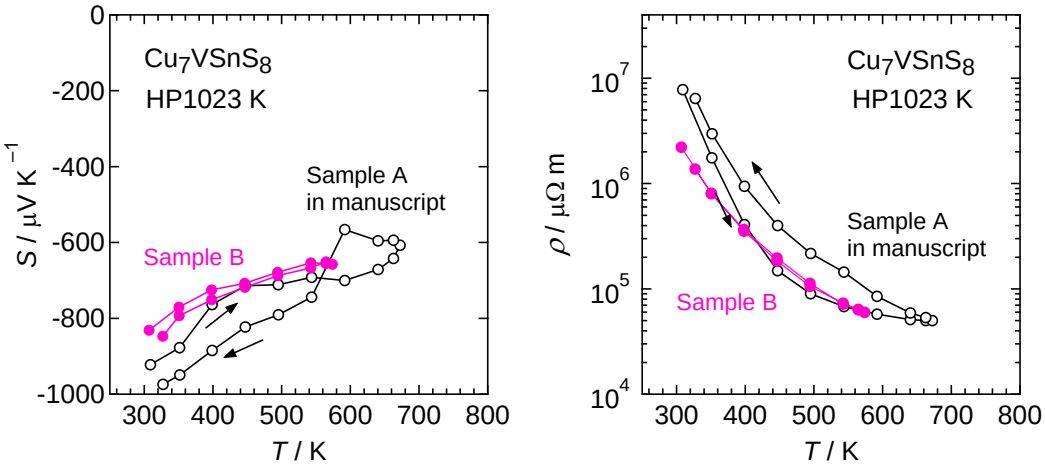

Fig. S7 N-type semiconducting behavior for the samples of Cu_7VSnS_8 hot-pressed at 1023 K.

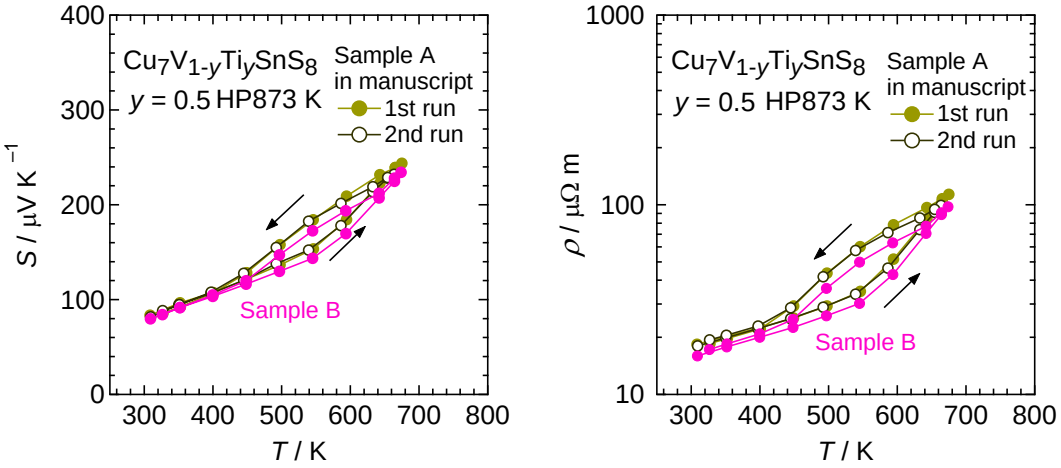

Fig. S8 Reproducibility of the data curve for the samples of $Cu_7V_{1-y}Ti_ySnS_8$ (y = 0.5) hot-pressed at 873 K.